Dynamics and Structure of Dusty Reacting Flows: Inert Particles in Strained, Laminar, Premixed Flames

FOKION N. EGOLFOPOULOS* and CHARLES S. CAMPBELL
Department of Aerospace and Mechanical Engineering, University of Southern California,
Los Angeles, CA 90089-1453

A detailed numerical study was conducted on the dynamics and thermal response of inert, spherical particles in strained, laminar, premixed hydrogen/air flames. The modeling included the solution of the steady conservation equations for both the gas and particle phases along and around the stagnation streamline of an opposed-jet configuration, and the use of detailed descriptions of chemical kinetics and molecular transport. For the gas phase, the equations of mass, momentum, energy, and species are considered, while for the particle phase, the model is based on conservation equations of the particle momentum balance in the axial and radial direction, the particle number density, and the particle thermal energy equation. The particle momentum equation includes the forces as induced by drag, thermophoresis, and gravity. The particle thermal energy equation includes the convective/conductive heat exchange between the two phases, as well as radiation emission and absorption by the particle. A one-point continuation method is also included in the code that allows for the description of turning points, typical of ignition and extinction behavior. As expected, results showed that the particle velocity can be substantially different than the gas phase velocity, especially in the presence of large temperature gradients and large strain rates. Large particles were also found to cross the gas stagnation plane, stagnate, and eventually reverse as a result of the opposing gas phase velocity. It was also shown that the particle number density varies substantially throughout the flowfield, as a result of the straining of the flow and the thermal expansion. Finally, for increased values of the particle number density, substantial flame cooling to extinction states and modification of the gas phase fluid mechanics were observed. As also expected, the effect of gravity was shown to be important for low convective velocities and heavy particles. Under such conditions, simulations indicate that the magnitude and direction of the gravitational force can substantially affect the profiles of the particle velocity, number density, mass flux, and temperature. © 1999 by The Combustion Institute

INTRODUCTION

Combustion science has been significantly advanced during the last 20 years mainly because of the evolution and extensive use of advanced laser diagnostics along with modeling made possible by supercomputers and the associated algorithms. Therefore, much has been learned in terms of the details of the underlying elementary processes of molecular transport and chemical kinetics as well as their interaction with the fluid mechanics. This knowledge, however, has been chiefly advanced in the gas phase, in which the assumptions of dilute gas can be a very good approximation, and many gas properties can be accurately determined from first principles. On the other hand, there is a wide range of combustion phenomena of interest in which the gas phase interacts in many different ways with a liquid or solid phase. While extensive work has been done on sprays, less attention has been given to the details of dusty reacting flows.

Dusty flows are of particular interest for a wide range of applications. Particles can be present in a gas intentionally or unintentionally, and they can be inert or reacting. Inert particles in an otherwise reacting gas flow can lead to flame cooling and modification of the extinction limits of a combustible mixture. Reacting solid particles can release substantial amounts of heat upon oxidation and can be used either for propulsion (e.g., Al, B, and Mg) or power generation (coal). Furthermore, accidents can occur when a reacting dust accumulates in air and which, in the presence of an ignition source, can cause explosion. Such explosions can occur during lumber milling, in grain elevators, and in mine galleries such as the one which occurred at the Haswell Colliery and resulted in the famous Faraday and Lyell report [1].

Particles are also used as seeds in reacting flows in order to measure flow velocities by using either the laser Doppler velocimetry

---

*Corresponding author. E-mail: egolfopo@alnitak.usc.edu

0010-2180/99/$–see front matter
PII S0010-2180(98)00110-2

COMBUSTION AND FLAME 117:206–226 (1999)
© 1999 by The Combustion Institute
Published by Elsevier Science Inc.

(LDV) or particle image velocimetry (PIV) techniques. The particles that are used in these applications must be chemically inert, so that they do not alter the chemical composition of the reacting stream. Furthermore, they must be small and light enough to closely follow the gas phase, in order to assure accurate gas-phase velocity measurements.

The addition of solid particles in a flowing gas stream can lead to strong couplings between the two phases, which can be of dynamic, thermal, and chemical nature. The dynamic coupling between the two phases is caused by the different inertia possessed by the fluid and solid phases, which results in slip between the phases that in turn can lead to the development of interphasial forces and the modification of the velocity fields of both phases. In addition to the phase-interaction forces, thermophoretic, centrifugal, electrostatic, magnetic, and gravitational field forces can be exerted on the particles. Of these, electrostatic and magnetic forces can generally be ignored as few combustors possess significant electrical and magnetic fields and centrifugal forces can be ignored unless strong flow rotation exists. On the other hand, thermophoretic forces, which are caused by steep temperature gradients, can be important in reacting dusty flows. The gravitational forces are unavoidably present and can play a substantial role in the overall dynamic response of the particle, especially for heavy particles. Indeed, existing experiments on dusty flows (e.g., [2]) indicate that global flame properties can be quite different when they are conducted at normal- and micro-gravity.

To understand the thermal effects of dust on combustion, it must be first realized that as the thermal capacity of the solid phase is of the order of 10^3 times that of the gas phase, it will respond more slowly to the temperature changes induced by the flame and, because the solid and gas phases are thermally coupled, slows the thermal response of the gas phase. Such temperature modifications can substantially affect the chemical kinetics of each phase. The thermal equilibration process will depend on the thermal properties of the two phases. Similarly, the emissivity of the solid phase is substantially higher compared to that of the gas phase so that the radiative transfer from the particles can result in significant energy losses.

The ultimate challenge of this type of research is to better understand the chemical coupling between the two phases. The problem is complicated because the actual mechanisms leading to particle gasification can differ depending on the chemical composition of the particle. For example, carbon burning initiates as a surface reaction that produces CO as a byproduct, which then diffuses from the surface and undergoes a secondary oxidation. Metal powders, such as Al, B, and Mg are first evaporated due to elevated temperatures and their vapor undergoes gas phase burning with the surrounding [3]. The chemical coupling between the two phases leads to particle size reduction, modification of the gas phase species composition, and the elevation of the temperature of both phases as a result of the exothermicity of both the surface and gas phase reactions. However, all particles begin this process as *inert* particles that must first be heated before they can themselves participate in the combustion process. Thus, one must first understand the more basic questions of the interactions of inert particles in a combustion environment before proceeding to the more complicated chemical effects.

The in-detail understanding of the dynamics and structure of heterogeneous (sprays or particle) flows can be only advanced by first considering simple flow geometries, which (1) can be conveniently produced in the laboratory, (2) can be simulated with the use of detailed description of all the all physico-chemical processes in both phases, and (3) are of relevance to practical turbulent reacting flows. Past experience in gas phase combustion has shown that the opposed-jet, stagnation-type flows are among the most meritorious and permit an in-depth understanding of the details of the pertinent physico-chemical processes.

A number of computational and experimental studies on sprays and particle flows (e.g., [4–12]) have been conducted in stagnation-type configurations. Numerically, the need for a hybrid Eulerian-Lagrangian approach has been identified by Continillo and Sirignano [4], and the use of such approach has allowed for the prediction of the phenomenon of droplet flow reversal [5, 6], which has been observed experimentally [7, 8]. Gomez and Rosner [9] have conducted a detailed study on the particle response in the opposed-jet configuration, and the particle thermophoretic diffusivities were determined experimentally. Sung, Law, and co-workers have conducted numerical studies [10, 11] on the effect of strain rate and temperature gradients on the dynamics of inert particles, as a way of understanding potential errors in experimental LDV data that might arise from thermophoretic forces that cause the motion of the tracer particles to differ from that of the gas. These studies have included the detailed description of the particle Stokes drag and thermophoretic forces. Results have shown that depending on the particle size, strain rate, and temperature gradient, the particle velocity can substantially differ from the gas phase velocity, which indeed compromises the fidelity of existing non-intrusive flow velocity measurement techniques. In these studies, the particle phase was not thermally coupled with the gas phase and was not allowed to affect the dynamics of the gas phase. Furthermore, the effect of gravity on the particle dynamics was not considered, since the focus of the study were the sub-micron sized particles, typically used as tracers, for which gravitational forces are negligible compared to fluid drag.

The behavior of reacting dusty flows can also have a strong dynamic and thermal dependence on the particle number density, n_p, which represents the number of solid particles per unit volume; such effects were not addressed in the previous numerical studies [10, 11]. Nonetheless, the values of n_p observed in a combustion environment will in most cases be very small. This can be easily seen by realizing that a stoichiometric mixture of volatile particles and oxidizer requires delivering masses of the same order of each to the flame, but since the density of the solid is roughly 3 orders of magnitude larger than that of the surrounding gas, the volumetric loading will be of the order of 10^{-3}. Consequently, it is unlikely that particles will interact with one another and modeling information derived from studies on single particles in infinite fluids may be used with confidence.

air

$C_{(s)} + O_2 + \frac{79}{21} N_2$

$\frac{V_c}{V_{air}} = \frac{12/\rho_{c(s)}}{144/\rho_{air}}$

$\sim 10^{-3}$

In view of the foregoing considerations, we have undertaken the task to conduct a long-term combined experimental and numerical study on the details of reacting dusty flows in which the effects of fluid mechanics, particle properties, steep temperature gradients, gas and particle detailed kinetics, and gravity are systematically addressed. Given the complexity that reacting particles introduce, in our first attempt to understand such complex phenomena, the dynamic, thermal, and gravitational effects were independently studied for the case of chemically inert particles; the term "inert" indicates that the particles are neither consumed nor they alter the gas phase chemistry. Thus in this paper, a systematic detailed numerical study is presented for inert particles embedded in strained, laminar premixed flames, which are stabilized in a stagnation-type flow configuration. Studies of chemically reacting particles will follow.

- not 3rd body.
- no quenching.

NUMERICAL APPROACH

Governing Conservation Equations

As mentioned in the Introduction, it is assumed that the particle number density is small enough so that the particles are very unlikely to encounter one another which greatly simplifies the governing equations. In describing the mechanics, we will consider both the solid and the gas phase. The gas includes both the original oxidizer and the gaseous species generated by the chemical reactions. The general steady conservation equations will be presented for the case of chemically inert particles in axisymmetric coordinates. Subsequently, these equations will be reduced to a quasi-one-dimensional formulation appropriate for the description of stagnation-type flows. In these equations, the subscripts "g" and "p" correspond to the gas and particle phase respectively.

The overall mass continuity equation for the gas phase is: steady state

$$\frac{1}{r}\frac{\partial(r\rho_g v_g)}{\partial r} + \frac{\partial(\rho_g u_g)}{\partial x} = 0 \qquad (1)$$

$\langle m_g \rangle$.

The gas phase steady momentum equations in the axial and radial directions are, respectively:

interphasial force

gravity

$$\rho_g u_g\left(\frac{\partial u_g}{\partial x}\right) + \rho_g v_g\left(\frac{\partial u_g}{\partial r}\right) = -\frac{\partial P}{\partial x} - \boxed{n_p F_{px}} + \frac{\partial}{\partial x}\left[\mu_g\left\{\frac{4}{3}\frac{\partial u_g}{\partial x} - \frac{2}{3r}\frac{\partial(rv_g)}{\partial r}\right\}\right] + \frac{1}{r}\frac{\partial}{\partial r}\left\{\mu_g r\left(\frac{\partial v_g}{\partial x} + \frac{\partial u_g}{\partial r}\right)\right\} + \boxed{\rho_g g} \tag{2}$$

$$\rho_g u_g\left(\frac{\partial v_g}{\partial x}\right) + \rho_g v_g\left(\frac{\partial v_g}{\partial r}\right) = -\frac{\partial P}{\partial r} + \boxed{n_p F_{PR}} + \frac{\partial}{\partial r}\left[\mu_g\left\{2\frac{\partial v_g}{\partial r} - \frac{2}{3}\frac{\partial u_g}{\partial x} - \frac{2}{3r}\frac{\partial(rv_g)}{\partial r}\right\}\right] + \frac{\partial}{\partial x}\left\{\mu_g\left(\frac{\partial v_g}{\partial x} + \frac{\partial u_g}{\partial r}\right)\right\} + \frac{2\mu_g}{r}\left(\frac{\partial v_g}{\partial r} - \frac{v_g}{r}\right). \tag{3}$$

In the above, equations, u and v represent the velocities in the axial (x) and radial (r) directions respectively, μ_g is the mixture dynamic viscosity, while n_pF_{PX} and n_pF_{PR} are the forces in the axial and radial directions, respectively, exerted upon a unit volume of gas by the particles [13] (the expressions for the forces exerted on each particle F_{PX} and F_{PR} in the axial and radial direction, respectively, will be given later in this section). The gravity term has been included only in the x-direction, which is parallel to the axis of symmetry of the counterflow.

The energy equation of the gas phase is given by

interphasial work done

$$r\rho_g u_g c_p\left(\frac{\partial T_g}{\partial x}\right) + r\rho_g v_g c_p\left(\frac{\partial T_g}{\partial r}\right) - \frac{\partial}{\partial x}\left(r\lambda_g\frac{\partial T_g}{\partial x}\right) - \frac{\partial}{\partial r}\left(r\lambda_g\frac{\partial T_g}{\partial r}\right) + r\rho_g\sum_{k=1}^{K} Y_k c_{pk} V_{kx}\frac{\partial T_g}{\partial x} + r\rho_g\sum_{k=1}^{K} Y_k c_{pk} V_{kr}\frac{\partial T_g}{\partial r} + r\sum_{k=1}^{K} h_k W_k \omega_k + Q_{g,rad} + n_p\left[\boxed{Q_p} + \boxed{(u_p - u_g)F_{PX} + (v_p - v_g)F_{PR}}\right] = 0 \tag{4}$$

Marble's interphasial heat xfer (cond. & conv.)

In the above equation, λ_g is the gas phase mixture conductivity, c_p is the mixture specific heat at constant pressure, c_{pk} is the specific heat at constant pressure of species k, Y_k is the mass fraction of species k, W_k is the molecular weight of species k, V_{kx}, and V_{kr} is the diffusion velocity of species k in the x and r direction respectively, h_k is the specific enthalpy of formation of species k, ω_k is the molar rate of production/destruction of species k resulting from all gas-phase chemical reactions, and K the total number of species. The term $Q_{g,rad}$ represents the gas radiative loss. The term Q_p represents the heat exchange (both by convection and conduction) between the particles and the gas phase. The terms $(u_p - u_g)F_{PX}$ and $(v_p - v_g)F_{PR}$ represent the work per unit time done by each particle against the F_{PX} and F_{PR} forces, respectively. For a reactive dusty flow, however, the heat release due to chemical reactions and the heat transfer because of steep temperature gradients dominate the contributions of the work terms so that $(u_p - u_g)F_{PX}$ and $(v_p - v_g)F_{PR}$ can be considered as negligible.

The gas radiation term $Q_{g,rad}$ is given at the optically thin limit by

$$Q_{g,rad} = 4\alpha_g\sigma(T_g^4 - T_u^4), \tag{5}$$

where σ is the Stefan-Boltzmann constant, T_u is the ambient temperature, and α_g is the total Planck's mean absorption coefficient of the gas.

Finally, the heat transfer term between one particle and the gas, Q_p, is given for low (≤ 1) particle Reynolds number, Re_p, by (e.g., [13]):

$$Q_p = 4\pi d_p\lambda_g(T_g - T_p), \quad [W] \tag{6}$$

where d_p is the particle diameter.

The conservation equation for the gas phase species k is

$$r\rho_g u_g\left(\frac{\partial Y_k}{\partial x}\right) + r\rho_g v_g\left(\frac{\partial Y_k}{\partial r}\right) + \frac{\partial}{\partial x}(r\rho_g Y_k V_{kx}) + \frac{\partial}{\partial r}(r\rho_g Y_k V_{kr}) - rW_k\omega_k = 0 \quad (7)$$

While the presentation of the gas phase equations above is an Eulerian one, the presentation of the particle equations in the following will be in Lagrangian terms. As first noticed by Continillo and Sirignano [4], this can be necessary for the simultaneous numerical integration of the gas and particle phase set of equations.

For the momentum balance equations for the particles, the formulation of Sung et al. [10, 11] was the starting point and appropriate modifications were introduced. In the absence of centrifugal, electrostatic and magnetic forces, the complete momentum balance for a single particle in the axial direction, is given in a Lagrangian frame of reference by:

$\langle u_p \rangle$

$$m_p\left(\frac{du_p}{dt}\right) = F_{PX} = F_{SDX} + F_{TPX} + F_{GRX}, \quad (8)$$

where m_p is the particle mass and is given by

$$m_p = \frac{\pi d_p^3}{6}\rho_{par} \quad (9)$$

and ρ_{par} is the density of the particle.

Not include

$\therefore \rho_{pa} \gg \rho_g$

Equation (8) does not include the terms representing forces due to the pressure gradient in the fluid, due to the fluid resistance to accelerating sphere, and due to the drag associated with unsteady motion. As Sung et al. [10, 11] have argued, these terms can be neglected as they are proportional to the gas density, which is much smaller than the particle density.

Not include

Equation (8) does not also include other phoretic effects such as diffusiophoresis, electrophoresis, and photophoresis [9]. Any effects of electrophoresis was not considered as the particles are not charged and no electric field is present. The effect of photophoresis was also ignored as it has been shown to have negligible contribution for conditions analogous to the ones studied herein [9]. The effect of diffusiophoresis was estimated by using the formulation recommended by Gomez and Rosner [9], given that our calculations were conducted for lean H$_2$/air flames. As species with very different molecular weights are present, the diffusiophoresis will be a function of the equivalence ratio, ϕ. It was found that its maximum value is 1.4 cm/s for the $\phi = 0.57$ and 0.4 cm/s for the leaner $\phi = 0.25$ hydrogen/air flames, the two cases studied herein. Given that these values constitute only a minor correction to the other types of velocities, the diffusiophoretic effect was not further considered.

1.5 100 $\frac{cm}{s}$

In Eq. (8), F_{SD} represents the Stokes drag force which owes its existence to the velocity slip between the two phases and is given for low (≤ 1) Re_p by (e.g., [10, 11]):

$$F_{SDX} = \frac{-3\pi\mu_g d_p(u_p - u_g)}{C(Kn)} \sim \frac{d_p(u_p-u_g)}{C(Kn)} \quad (10)$$

This corresponds to the Type III approximation of Hjelmfelt and Mockros [14] with the addition of a slip correction factor C, which is needed in order to modify the Stokes' law for the sub-μm seeding particles. The Knudsen-Weber expression for C and for all Knudsen numbers is (e.g., [10, 11]):

$$C = 1 + Kn[\alpha + \beta \exp(-\gamma/Kn)], \quad (11)$$

where α, β, and γ are constants derived from the fitting of the Knudsen-Weber formula to the experimental data and are equal to 1.142, 0.558, and 0.999, respectively [15]. The particle Knudsen number is defined as $\boxed{Kn = 2l_{fp}/d_p}$ where l_{fp} is the mean free path of the gas molecules given by $\mu_g = \Phi\rho_g l_{fp} c_{mg}$ (e.g., [16, 17]) where Φ is a constant equal to 0.491, and c_{mg} is the mean velocity of the gas molecules. Assuming that the molecules follow a Maxwell distribution, c_{mg} is given by (e.g., [17]):

$$c_{mg} = (8k_{BOLTZ}T_g/\pi m_g)^{1/2}. \quad (12)$$

In Eq. 12, k_{BOLTZ} is the Boltzmann constant and m_g is the reduced molecule mass. For a multicomponent mixture m_g is given by

$$\frac{1}{m_g} = \sum_{k=1}^{K}\frac{1}{m_{g,k}}. \quad (13)$$

where

$$m_{g,k} = \frac{W_k}{N_{\mathrm{Avogadro}}} \tag{14}$$

with N_{Avogadro} being the Avogadro constant.

As mentioned earlier, Eq. 10 is applicable only for very low Re_p numbers. It was one of the goals of the present study, however, to investigate cases in which the particles' Re_p is larger compared to the studies of Sung et al. [10, 11]. Thus, a correction was introduced to Eq. 10 (e.g., [18]):

$$F_{SDX} = \frac{-3\pi\mu_g d_p(u_p - u_g)}{C}(1 + 0.15Re_p^{0.687}), \tag{15}$$

where Re_p is defined as

$$Re_p = \frac{\rho_g d_p|(u_p - u_g)|}{\mu_g}. \tag{16}$$

It should be noted in passing, that the relative velocity between the gas and particle phase is the appropriate characteristic velocity to use in the definition of Re_p. Results showed that this correction could play an important role on the particle dynamic behavior as Re_p increases.

The term F_{TPX} represents the thermophoretic force on a spherical particle due to gas phase temperature gradient ∇T_g. In the near-continuum limit, F_{TPX} is given from Brock [19]:

$$F_{TPX} = \frac{-6\pi\mu_g\eta_g d_p C_s\left(\frac{\lambda_g}{\lambda_p} + C_t Kn\right)\frac{\nabla T_g}{T_g}}{(1 + 3C_m Kn)\left(1 + 2\frac{\lambda_g}{\lambda_p} + 2C_t Kn\right)}, \tag{17}$$

where $\eta_g = \mu_g/\rho_g$, and C_m, C_s, and C_t constants with values 1.14, 1.17, and 2.18, respectively [20], which assure that the fitting formula covers satisfactorily the entire range of Kn numbers. In the work of Talbot, Cheng, Schefer, and Willis [20], this is justified by realizing that Eq. 17 degenerates within 3% to the collisionless limit (i.e., as $Kn = 2l_{fp}/d_p \to \infty$) given by Waldmann [21]. The thermophoretic force F_{TPX} is included because of its significance in reacting flows, in which particles with diameters of the order of microns are flowing against substantial temperature gradients. Then, the thermophoretic force has a direction pointing from the high gas temperatures towards the low gas temperatures and opposes the particle motion towards the flame (e.g., [9]).

The term F_{GRX} represents the gravitational force on each particle and is given by:

$$F_{GRX} = -m_p g, \tag{18}$$

where g is the prevailing gravitational acceleration. In the present investigation various values of g were used, in order to systematically study the effect of gravity. Under normal gravity conditions, $g = +981.0$ cm/s^2 for cases in which gravity opposes the particle motion ($+g$ case), and $g = -981.0$ cm/s^2 for cases in which gravity favors the particle motion ($-g$ case). Baseline studies were also performed at zero gravity $g = 0$ (0-g case).

For a vertically oriented stagnation flow configuration in which all flame properties are radially uniform, the complete momentum balance for a single particle in the radial direction is given in a Lagrangian frame of reference by

$$m_p\left(\frac{dv_p}{dt}\right) = F_{PR} = F_{SDR}, \tag{19}$$

where

$$F_{SDR} = \frac{-3\pi\mu_g d_p(v_p - v_g)}{C}. \tag{20}$$

In Eq. 20, Re_p number corrections similar to the ones introduced in Eq. 15 are not required, given that around the centerline the velocities v_p and v_g are very small and their difference results in low Re_p.

In order to reduce the system of the gas phase equations from the axisymmetric to a quasi-one-dimensional formulation similarly to Kee et al. [22], the quantities n_p, u_p, and F_{PX} must be considered as functions of x only. In the ideal case of a strictly planar boundary layer between two opposed jets, this formulation describes the flow throughout the spatial domain between the two jets. In realistic experiments, however, obtaining planar geometry throughout is not possible given that "edge" effects result from the unavoidable shear, which develops between the counterflowing jets and the ambient stagnant or coflowing gas. Furthermore, the experimental flames always have a minor curvature around the centerline, which is result of the pressure gradients which develop in the stagnation flow and which can affect the flatness of nozzle exit velocity, u_{exit}. Under such realistic conditions, the quasi-one dimensional formulation is a valid approximation at least in the immediate vicinity of the centerline of the system, as the symmetry requirement imposes that radial gradients must be zero asymptotically close to the centerline. Furthermore, Eqs. 19 and 20 can be combined to

$$m_p v_p\left(\frac{\mathrm{d}v_p}{\mathrm{d}r}\right) = \frac{-3\pi\mu_g d_p(v_p - v_g)}{C}$$

and by dividing both sides by r

$$m_p \frac{v_p}{r}\left(\frac{\mathrm{d}v_p}{\mathrm{d}r}\right) = \frac{-3\pi\mu_g d_p}{C}\left(\frac{v_p}{r} - \frac{v_g}{r}\right)$$

or

$\langle V_p \rangle$

$$m_p G_p G_p = \frac{-3\pi\mu_g d_p}{C}(G_p - G_g). \tag{21}$$

Equation 21 was derived based on the fact that the radial velocities of both the gas and the particle must vary linearly with r, as a result of a Taylor's expansion asymptotically around the centerline (small r). The quantities G_g and G_p have been defined as

$$G_g \equiv \frac{v_g}{r} = \frac{\partial v_g}{\partial r}$$

and

$$G_p \equiv \frac{v_p}{r} = \frac{\partial v_p}{\partial r} \tag{22}$$

and are functions of x only, i.e., $G_g = G_g(x)$ and $G_p = G_p(x)$.

The analysis conducted by Kee et al. [22] shows that if all properties are only a function of x then by differentiating the x-momentum equation with respect to r and the r-momentum equation with respect to x, the pressure curvature $J_g \equiv (1/r)(\partial P/\partial r)$ emerges as an eigenvalue of the problem. In Ref. 22, gravity was not included. If the gravity term $\rho_g g$ is included in the x-momentum equation, and given that this term is only a function of x, at least asymptotically around the centerline, it can be easily shown that J_g remains an eigenvalue of the problem. Thus, the reduced quasi-one-dimensional gas phase mass continuity becomes

$$2\rho_g G_g - \frac{\mathrm{d}(\rho_g u_g)}{\mathrm{d}x} = 0. \tag{23}$$

$\langle \rho_g \rangle$

The reduced quasi-one-dimensional radial momentum equation for the gas phase becomes:

$$\rho_g u_g\left(\frac{\mathrm{d}G_g}{\mathrm{d}x}\right) + \rho_g G_g^2 - J_g - \frac{\mathrm{d}}{\mathrm{d}x}\left[\mu_g \frac{\mathrm{d}G_g}{\mathrm{d}x}\right] - n_p \frac{3\pi\mu_g d_p(G_p - G_g)}{C} = 0. \tag{24}$$

$\langle V_g \rangle$

It should be noted that while Eq. 23 is identical to the one derived for the gas phase stagnation flow [22], Eq. 24 is modified through the addition of the last term in the left-hand side, which accounts for the gas-particle forces.

It is important to emphasize that the presence of gravity does not affect the u_g velocity profile along the centerline. This a result of the requirement that gravity acts only in the x-direction and that radial symmetry must prevail at least around the centerline. Thus, for a given set of boundary conditions for u_{exit} at the two ends of the finite domain, G_g is determined through the radial momentum Eq. 24 while u_g is determined from the gas phase mass continuity Eq. 23. Gravity, however, alters the axial variation of the hydrodynamic pressure through the $\mathrm{d}P/\mathrm{d}x$ term, which has to be modified at the exits of the two nozzles in order to maintain the u_{exit} values imposed as boundary conditions. This physically compensates for the presence of gravitational forces. This analysis is only valid either for the ideal case of infinitely large nozzles resulting in strictly planar geometry, or at least around the centerline for the more relevant case of finite-size nozzles.

The quasi-one-dimensional energy equation for the gas phase becomes

$$\rho_g u_g c_p\left(\frac{\mathrm{d}T_g}{\mathrm{d}x}\right) - \frac{\mathrm{d}}{\mathrm{d}x}\left(\lambda_g \frac{\mathrm{d}T_g}{\mathrm{d}x}\right) + \rho_g \sum_{k=1}^{K} Y_k c_{pk} V_{kx} \frac{\mathrm{d}T_g}{\mathrm{d}x} + \sum_{k=1}^{K} h_k W_k \omega_k + Q_{g,\text{rad}} + n_p Q_p = 0. \tag{25}$$

$\langle T_g \rangle$

In Eq. 25, $Q_{g,rad}$ is given by Eq. 5, while the particle-gas heat transfer was accounted for larger Re_p's by using a correction factor C_{NU}:

$$Q_p = 4\pi d_p \lambda_g (T_g - T_p) C_{NU}. \tag{26}$$

C_{NU} is a function of Re_p that reflects the way that the Nusselt number increases with Re_p and was determined as a function of ln (Re_p) by fitting a 4th-order polynomial to the experimental results reported by Clift, Grace, and Weber [23]. This correction is essential when studying large particles that typically operate at Re_p's larger than one.

The quasi-one-dimensional conservation equation for the gas phase species k is given by

$\langle Y_K \rangle$

$$\rho_g u_g \left(\frac{dY_k}{dx} \right) + \frac{d}{dx} (\rho_g Y_k V_{kx}) - W_k \omega_k = 0. \tag{27}$$

The formulation of the thermal energy equation for a single particle was based on the assumption that the particle temperature is uniform and is a function of time only. This is a valid assumption for small particles as long as the solid conductivity is much larger than that of the gas. Thus, the particle thermal energy equation is given in a Lagrangian frame of reference by

$\langle T_P \rangle$

$$m_p c_{par} \left(\frac{dT_p}{dt} \right) - Q_p + Q_{p,rad} - Q_{g,rad-p} = 0. \tag{28}$$

The term Q_p is given by Eq. 26. The term $Q_{p,rad}$ is the radiative heat loss emitted from the particle surface and is given by

$$Q_{p,rad} = A_p \epsilon_p \sigma (T_p^4 - T_u^4), \tag{29}$$

where c_{par} is the particle specific heat, ϵ_p is the particle emissivity, and $A_p = \pi d_p^2$ is the surface of the (spherical) particle.

The term $Q_{g,rad-p}$ represents the thermal energy, which is emitted by the gas phase and eventually is absorbed by each particle. In evaluating this term, each particle at any spatial location was allowed to absorb heat that is radiated from every point in the gas phase. The heat absorption was determined by dividing the gas into layers parallel to the flame and then computing the radiative flux using a configuration factor for exchange between a circular disk, representing the gas layer, and a sphere, representing the particle [24]. Subsequently, $Q_{g,rad-p}$ was determined by summing the absorbed energy from all gas layers.

The mass conservation of the particles is described in an Eulerian frame of reference by

$$2\rho_p G_p + \frac{d(\rho_p u_p)}{dx} = 0,$$

where $\rho_p \equiv n_p m_p$. For constant m_p:

$$2n_p G_p + \frac{d(n_p u_p)}{dx} = 0. \tag{30}$$

Eq. 30 can be written in a Lagrangian frame of reference as:

$G_p = \frac{\partial U_p}{\partial r}$

$$2n_p G_p + \frac{d(n_p |u_p|)}{ds} = 0, \tag{31}$$

where s is the coordinate which specifies the Lagrangian distance traversed by a particle since injection; as the particle may reverse direction during its flight, it can pass through the same Eulerian point, x, many times and its properties at that point can be multiple-valued. However, the total Lagrangian distance s, will steadily increase with time. Note that the velocity in the direction of s is the absolute value of the Eulerian velocity $|u_p|$. The use of s allows for the tracking of n_p which becomes singular wherever the particles undergo path reversal. The following integration of Eq. 31 results in a formula in which the solid properties will be single-valued as functions of s:

$$n_p = n_{p,inj} \exp \left[- \int_0^t \left(2G_p + \frac{d|u_p|}{ds} \right) dt \right]$$

$$= n_{p,inj} \exp \left(- \int_0^t 2G_p \, dt \right)$$

$$\cdot \exp \left(- \int_0^t \frac{d|u_p|}{ds} dt \right).$$

Given that

$$\int_0^t \frac{d|u_p|}{ds} dt = \int_0^s \frac{d|u_p|}{ds} \frac{ds}{|u_p|}$$

$$= \int_{|u_{p,inj}|}^{|u_p|} d \ln |u_p| = \ln \left(\frac{|u_p|}{|u_{p,inj}|} \right)$$

and

$$\exp\left[-\ln\left(\frac{|u_{\mathrm{p}}|}{|u_{\mathrm{p,inj}}|}\right)\right] = \frac{|u_{\mathrm{p,inj}}|}{|u_{\mathrm{p}}|},$$

then

$\langle S_p \rangle$

$$n_{\mathrm{p}} = n_{\mathrm{p,inj}} \frac{|u_{\mathrm{p,inj}}|}{|u_{\mathrm{p}}|} \exp\left(-\int_0^t 2G_{\mathrm{p}}\,\mathrm{d}t\right), \qquad (32)$$

where $n_{\mathrm{p,inj}}$ and $u_{\mathrm{p,inj}}$ are the particle injection number density and velocity, i.e., their respective values at the nozzle exit.

A analogous approach for the determination of n_{p} for droplets across singular reversal points has also been taken successfully by Gutheil and Sirignano [6], who studied the droplet behavior by dividing the computational domain in "sheets," with each sheet corresponding to a droplet path between reversal points. Furthermore, a rigorous mathematical explanation has been provided, which also proves that this singularity is an integrable one.

It is essential that an important clarification is made on the definition of the number density n_{p}, in cases where there are length scales in the flow direction (i.e., the flame thickness), which are of the same size as the particles. The number density is technically defined as the number of particles counted in a volume, in the limit where the volume goes to zero. Presumably, that volume cannot get smaller than a particle diameter, but does that mean that n_{p} is meaningless over such scales? The answer is largely one of definition of the averaging volume and is not a problem for the present study where the conditions are steady at each Eulerian point. Under such a condition, the extent of the averaging in the direction of the flow (the direction for which the flame thickness is a relevant scale) can be defined as the flow velocity multiplied by a short period of time and can take that limit as the time goes to zero. Note that this is not a redefinition of n_{p} as, because the system is statistically stationary, it is exactly the same as making a volume average. Furthermore, it should be clear that when n_{p} is understood in this sense, there is no change in the meaning of any of the mass conservation equations presented above, which is the critical issue.

In summary, the gas phase is governed by Eqs. 23, 24, 25, and 27 while the particle phase is governed by Eqs. 8, 21, 28, and 32.

Description of Singular Points Through One-Point Continuation

The injection of particles in flames can result in substantial modification of the properties of the gas phase: for example, the large heat capacity of the particles dictates that they heat more slowly than the surrounding gas. If the injected number density $n_{\mathrm{p,inj}}$ is large enough, this cooling may lead to flame extinction. As a result, a turning point behavior can be expected [25] under certain conditions in a flame temperature vs $n_{\mathrm{p,inj}}$ diagram. Such turning-point behavior cannot be determined through varying $n_{\mathrm{p,inj}}$, as the extinction point is singular. This can be resolved by following the continuation approach of Nishioka et al. [26]. Thus, a one-point continuation approach was implemented by imposing a predetermined gas-phase temperature reduction at one point within the flow field, so that the $n_{\mathrm{p,inj}}$ would become part of the solution, and its respective injection (initial) value was removed. The internal point was chosen to be the location at which the temperature has maximum slope, following the recommendations of Nishioka et al. [26]. In the present study the one-point continuation approach was applied for the determination of $n_{\mathrm{p,inj}}$. However, this approach can be easily extended to study extinction and/or ignition as functions of the particle temperature, diameter, or any other physical property of the solid phase.

Physical and Chemical Properties

In the present investigation, the response of inert Al_2O_3 particles were studied as a model case in premixed, atmospheric, lean H_2/air flames by including detailed descriptions of chemical kinetics and molecular transport.

The hydrogen kinetics were taken from the GRI 2.1 kinetic mechanism [27], and the molecular properties pertinent to the calculation of transport coefficients were taken from the Sandia Transport Package code [28].

For the calculation of the gas phase radiative heat transfer, the total Planck's mean absorption coefficient, α_{g}, was calculated based on the H_2O. The Planck mean absorption coefficient α_{H_2O} for H_2O is given for optically thin conditions by Tien [29] and Hubbard and Tien [30] as functions of temperature. Then, the total mean absorption coefficient, α_g is given by

$$\alpha_g = \alpha_{H_2O} p_{H_2O}, \qquad (33)$$

where p_{H_2O} is the partial pressure of H_2O. More details on the formulation of the gas radiation can be found in [31, 32].

The physical properties for the Al_2O_3 particles were taken from Rosenhow, Hartnett, and Ganic [33]. The particle heat capacity, c_{par}, and thermal conductivity, λ_p, were fitted as functions of the particle temperature by using 5th-order polynomials. The density of the Al_2O_3 was taken as ρ_{par} = 3.97 g/cm^3 and the particle emissivity as ϵ_p = 0.25 [33].

Method of Solution

The steady conservation equations for both the gas and particle phases were simultaneously solved by modifying an existing stagnation-flow code [34], which had been used to solve steady and unsteady premixed and non-premixed counterflowing flames.

The gas phase equations were solved in a manner similar to the Sandia flame codes by using a damped Newton method. In terms of boundary conditions, the reactant, velocity, temperature (always 300 K), and concentrations at the nozzles' exits were specified. Furthermore, plug flow conditions were assumed at the nozzle exits. More specifically, the gas phase velocity gradients were set equal to zero, although relaxation of such conditions is not expected to alter the underlying physics of the problem. The code was integrated into the CHEMKIN [35] and Transport [28] subroutine packages.

particle
8 $\langle u \rangle$
21 $\langle v \rangle$
28 $\langle T \rangle$
32 $\langle g \rangle$

The particle conservation Eqs. 8, 28, and 31 are first-order differential equations and can be marched in time (space) by using only one initial (boundary) condition, respectively. The radial momentum Eq. 21, is algebraic so that G_p can be computed directly without any initial or boundary conditions. As first noticed by Continillo and Sirignano [4], the time-marching, Lagrangian approach for solving Eqs. 8, 28, and 31 is preferable given that, under certain conditions, the space-marching, Eulerian approach cannot handle singular behaviors in space which may not be singular in time. This happens when the particles undergo flow reversal. This is possible when a particle's inertia forces it to cross the gas stagnation plane (GSP), and penetrate into a counterflowing gas stream, which eventually forces stagnation and reversal of the particle stream.

initially
$\langle \ \rangle_p = \langle \ \rangle_g$

For the Lagrangian solution of the particle equations, the velocity and temperature of the particles were set to be equal to these of the gas phase at the nozzle exits (t = 0). Relaxation of these assumptions is, again, not expected to alter the physics of the problem. The Lagrangian, time marching was subsequently conducted with variable time steps, Δt. It was found that it was beneficial to adjust the time step Δt so that the spatial locations resulting from the Lagrangian marching would coincide with the spatial locations as determined by the Eulerian solution procedure for the gas phase. Thus, the need for spatial interpolations, which inherently introduce inaccuracies, was eliminated.

Eulerian
→ Lagrangian
no
interpolation

During the Lagrangian time-stepping, the particle axial momentum Eq. 8 was first advanced to a new time step so that the new u_p was determined. During the solution of Eq. 8, an iterative procedure was followed which would converge to the correct value of u_p starting from a reasonable initial guess. This was needed because of the existence of the Re_p number term in the Stokes drag force as given by Eq. 15. Having determined the new u_p value, the particle thermal energy Eq. 28 was then advanced for the determination of the value of T_p at the new time step. Similarly to the particle axial momentum equation, an iteration scheme was also needed given that the fourth power of T_p is involved in the $Q_{p,rad}$ term, and a closed form solution cannot be directly obtained. The G_p was determined directly at all times from the algebraic Eq. 21. Subsequently, the particle number density Eq. 31 was advanced through the analytical expression, Eq. 32. It should be noted that while the behavior of Eq. 32 is singular at the locations of particle flow reversal at which u_p = 0, its integration just before and just after the singular point can be conveniently done as G_p is finite throughout the particle's Lagrangian path.

RESULTS AND DISCUSSION

The interactions between the inert particles and a reacting gas phase can be both dynamic and thermal, and they are controlled by a number of parameters which have to be varied independently. These parameters are the gas phase injection velocity (which controls the strain rate) and chemical composition, and the particle injection velocity, diameter, and number density. Since the present study was conducted for Al_2O_3 particles only, the physical properties of the particles were fixed. Otherwise, these properties can be also independently varied.

The numerical simulations were conducted for opposed-jet, atmospheric, laminar premixed H_2/air flames, with a nozzle separation distance of 1.4 cm (left nozzle located at $x = -0.7$ cm and right nozzle at $x = +0.7$ cm) and for $\phi = 0.57$ and 0.25. The nozzle exit velocities, u_{exit}, of the gas and particle phases were identical for both nozzles and varied from as low as 14 cm/s to as high as 800 cm/s.

The twin-burner assembly was considered to be vertical so that the gravitational forces would act along the direction of the system centerline. Given the unidirectional nature of gravity, its effect on the particle dynamics was considered for three cases. The first case was that of $(+g)$ in which the particles were injected from the bottom nozzle with the gravity opposing the particle axial motion. The second case is that of $(-g)$ in which the particles were injected from the top nozzle with the gravity favoring the particle axial motion. The third case is that of zero gravity $(0\text{-}g)$. The $(+g)$ and $(-g)$ conditions can be easily produced in the laboratory under normal gravity conditions. The $(0\text{-}g)$ conditions can and will be produced in special NASA facilities such as a drop tower and/or a parabolic-trajectory aircraft.

In all figures which follow, the particles were injected from the left nozzle at a spatial location $x = -0.7$ cm with a direction from left to right. By injecting particles from one nozzle only, an asymmetry was imposed to the system. This was intentional as it allows for the possibility of particle penetration into the opposing side of the GSP which leads to a variety of dynamic and thermal phenomena. In the previous studies of Sung et al. [10, 11] only small particles were studied, which nearly follow the gas phase and always stagnate closely to the GSP. It should be finally noted, that in the present calculations two identical premixed flames are symmetrically established, one on each side of the GSP.

In the present study, the particle diameters were varied from 0.3 to 100 μm which is the range of interest for our scheduled experiments. Finally, the injection number density at the nozzle exit, $n_{p,inj}$, was varied from values as low as 10 particles/cm^3 to values high enough to cool the flame and eventually cause local and global extinction.

Dynamic Effects on the Particles

The particles' dynamic response is chiefly controlled by its momentum through Eqs. 8 and 21. Equation 8 can be easily transformed to an Eulerian frame of reference, and by dividing both sides by $u_p m_p$ and by realizing that m_p is proportional to $(d_p)^3$ it can be shown that the spatial variation of u_p is given by

$$\frac{du_p}{dx} = \overset{\text{Stoke}}{\frac{A_1}{u_p d_p^2}(u_g - u_p)} + \overset{\text{thermophoretic}}{\boxed{\frac{A_2}{u_p d_p^2}}\frac{\nabla T_g}{T_g}} + \frac{g}{u_p}, \text{ gravity} \quad (34)$$

where A_1 and A_2 are combinations of various parameters contained in Eqs. 15 and 17. A careful inspection of Eq. 34 reveals that as d_p increases the contribution of the thermophoretic force is reduced. The Stokes drag remains important, as a larger d_p implies larger particle inertia, which can lead to larger velocity difference $(u_g - u_p)$ and which partially offsets the effect of the diameter in the denominator. Equation 34 also reveals that as u_p increases, the thermophoretic contribution is also reduced. Similarly to the previous case, an arbitrarily large u_p can result in large slip velocities $(u_g - u_p)$. Thus, the effect of thermophoresis is expected to be important for small particles and low particle velocities. A comparison between the Stokes drag and the gravity term reveals that the gravitational force will be important for large particles and low particle velocities, as expected.

$\frac{S}{m_p} \sim \frac{d^2}{d^3} \sim \frac{1}{d}$.

$g = const.$

Stokes drag and thermophoretic effects

The effects of Stokes drag and thermophoresis are demonstrated in Fig. 1, which depicts the u_p profiles of 0.3 and 5.0 μm particles respectively

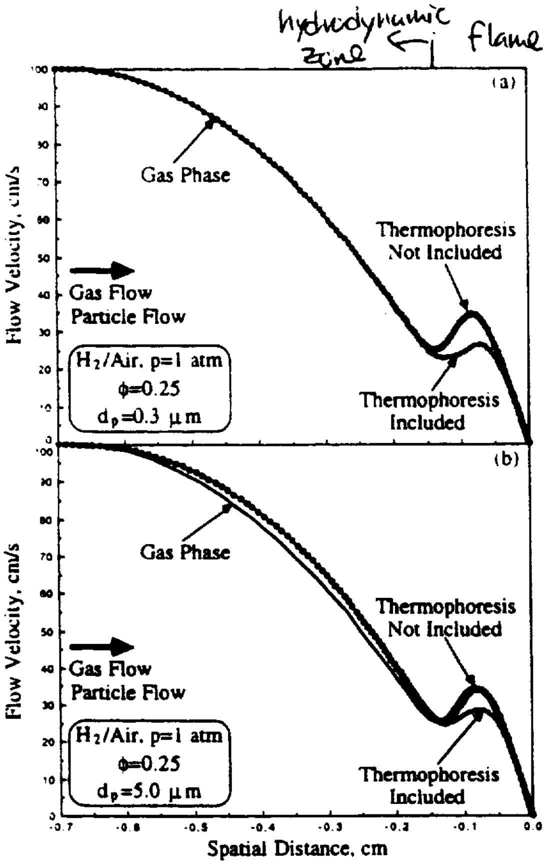

Fig. 1. Gas phase and particle axial velocities profiles for a $\phi = 0.25$ H_2/air flame with $u_{exit} = 100$ cm/s, $n_{p,inj} = 10$ particles/cm^3, and (a) $d_p = 0.3$ μm and (b) $d_p = 5.0$ μm with and without the inclusion of thermophoresis. Simulations also included the contributions of Stokes drag and normal gravity ($+g$).

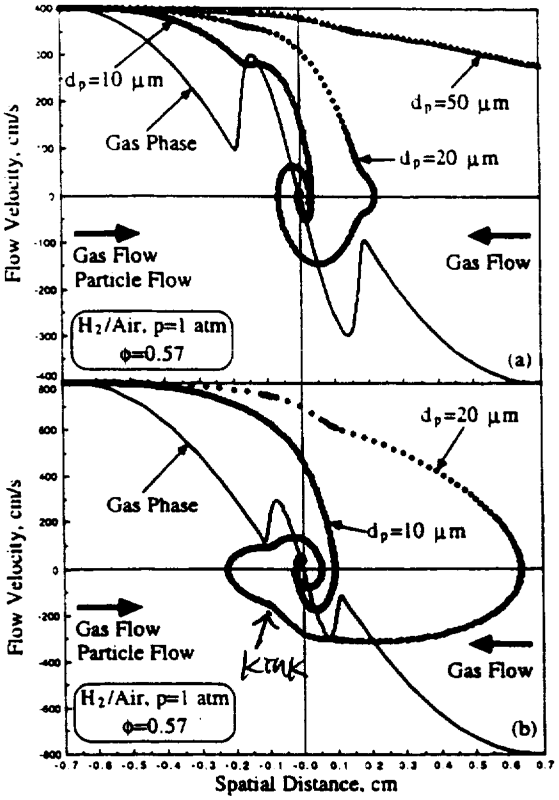

Fig. 2. Gas phase and particle axial velocities profiles for a $\phi = 0.57$ H_2/air flame with $n_{p,inj} = 10$ particles/cm^3, for (a) $u_{exit} = 400$ cm/s and $d_p = 10$, 20, and 50 μm and (b) $u_{exit} = 800$ cm/s and $d_p = 10$ and 20 μm. Simulations included the contributions of Stokes drag, thermophoresis, and normal gravity ($+g$).

for the $\phi = 0.25$ flame. Results indicate that for $d_p = 0.3$ μm, the particles follow closely the gas phase in the hydrodynamic zone and that inside the flame zone a substantial velocity difference develops between the two phases. This difference was found to be larger for the weaker $\phi = 0.25$ flame in which the extent of the thermal expansion and the resulting gas phase velocities in this expansion zone are lower compared to the stronger $\phi = 0.57$ flame. For the larger 5.0 μm particles, it can be seen that the increased inertia of the particles results in a substantial difference between u_p and u_g even in the decelerating hydrodynamic zone. Calculations were also conducted without accounting for the effect of the thermophoresis and the results are also shown in Fig. 1. It is apparent that thermophoresis is chiefly responsible for the discrepancy between u_g and u_p within the thermal expansion zone and that by neglecting F_{TPX}, u_p closely follows u_g. These observations are consistent with similar previous studies (e.g., [10, 11]).

Typically, both the 0.3 and 5.0 μm particles used to generate the data in Fig. 1 possess small particle inertia as is desirable for tracer particles used in LDV and PIV measurements, and Fig. 1 shows that these particles can closely follow the gas phase and, in particular, that they reach zero velocity at the GSP. By further increasing the particle inertia, which may be accomplished either by increasing the injection velocity and/or the particle diameter, it is possible that the particles will penetrate the GSP of the gas phase and stagnate at a different location, defined as the particle stagnation plane (PSP). This is illustrated in Fig. 2 for the $\phi = 0.57$ flame for $u_{exit} = 400$ and 800 cm/s, respectively, and for various particle sizes. Figure 2a depicts that for u_{exit} = 400 cm/s, the 10 and 20 μm particles penetrate the GSP, and stagnate within the region of the opposing jet emerging from the upper burner. This leaves them with zero velocity in a region of reversed gas flow. Consequently, the particles reverse direction and again cross the GSP where they may stagnate again and undergo a subsequent reversal. This results in an oscillating motion, but one that is strongly damped, so that the particles eventually stagnate on the GSP. This oscillatory behavior has been previously observed for droplets [5, 6, 8] and particles [7] in stagnation flow configurations. The results of Fig. 2a indicate that the 20 μm particles penetrate deeper into the opposing jet regime than do the 10 μm particles because of their increased inertia, while the 50 μm particles have a high enough inertia to reach all the way to the opposing nozzle exit. The results of Fig. 2b for the higher u_{exit} = 800 cm/s indicate that the 20 μm particles reach much deeper into the opposing jet regime compared to the u_{exit} = 400 cm/s case, and they undergo the first reversal at a location very close to the exit of the opposing nozzle. Note that "kinks" can be observed in the 20 μm curves for both injection velocities; for the u_{exit} = 400 cm/s line, the kink can be observed on the first reversal point on the right hand side of the GSP, while for the u_{exit} = 800 cm/s line, the kink can be seen at the second reversal point on the left side of the GSP. These kinks correspond to the points where the particles pass through the thermal expansion zones which surround the flames on either side of the GSP. Notice that, at those points, the gas undergoes a rapid acceleration in response to the intense heating. Thus, if the particles can pass through the flames, they enter into a regime of reduced gas velocity within which they decelerate much more slowly. The kinks observed in Fig. 2 are a result of this rapid change in deceleration rate.

Number density effects

The variation of the particle number density, n_p, was also studied for a wide range of conditions. These studies show certain peculiarities especially around the PSP where the axial term of Eq. 31 becomes singular. Our method of dealing with the singular behavior was discussed in the Numerical Approach section.

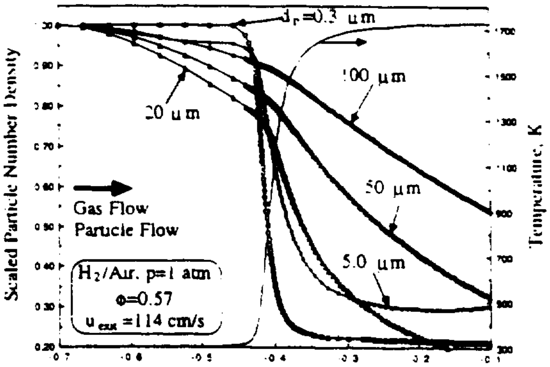

Fig. 3. Profiles of scaled by its injection value particle number density for a ϕ = 0.57 H_2/air flame with u_{exit} = 114 cm/s, $n_{p,inj}$ = 10 particles/cm^3, and d_p = 0.3, 5.0, 20, 50, and 100 μm. Simulations included the contributions of Stokes drag, thermophoresis, and normal gravity ($+g$). Temperature profile (solid line) indicates flame location.

The spatial variation of n_p, scaled by $n_{p,inj}$, is shown in Fig. 3 for the ϕ = 0.57 flame, u_{exit} = 114 cm/s, and particle diameters 0.3, 5.0, 20, 50, and 100 μm. Note that only the region to the left of the GSP is shown in this figure. For the 0.3–20 μm particles, it can be seen that n_p is characterized by three distinct slopes. In the hydrodynamic region of the flow, it is constant or decreases slowly. It then undergoes a rapid reduction within the thermal expansion region and subsequently, this reduction becomes milder. The rapid reduction in the thermal expansion region can be understood as the gas stream undergoes a rapid acceleration there, which induces an acceleration of the particle stream; the reduction is then explained as Eq. (32) indicates that $n_p/n_{p,inj}$ varies inversely to u_p. However, the inertia of the 50 and 100 μm particles is large enough to make them immune to all of these effects, and their velocities seem to decrease with a nearly-constant slope, which is somewhat affected by the thermal expansion. The results of Fig. 3 also indicate that the slope of n_p in the hydrodynamic zone has a non-monotonic dependence on d_p which can be attributed to the competition between the G_p and $d(u_p)/dx$ terms. More specifically, it becomes steeper as d_p increases from 0.3 to 20 μm, and it becomes milder as d_p further increases to 50 and 100 μm.

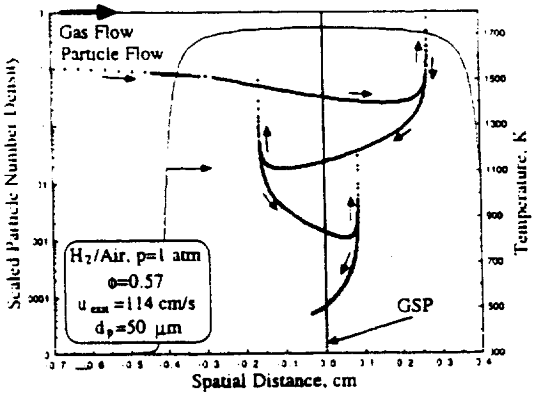

Fig. 4. Profiles of scaled by its injection value particle number density for a $\phi = 0.57$ H_2/air flame with $u_{exit} = 114$ cm/s, $n_{p,inj} = 10$ particles/cm^3, and $d_p = 50$ μm. Simulations included the contributions of Stokes drag, thermophoresis, and normal gravity ($+g$). Arrows indicate the direction of the particle motion. Temperature profile (solid line) indicates flame location.

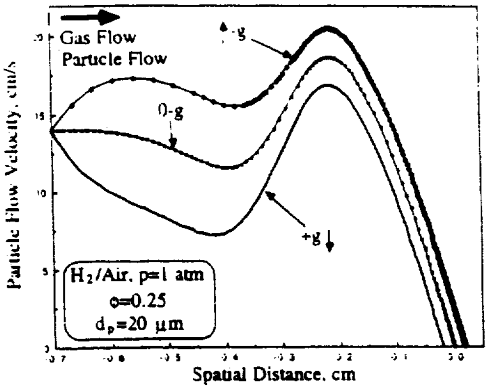

Fig. 5. Gas phase and particle axial velocities profiles for a $\phi = 0.25$ H_2/air flame with $u_{exit} = 14$ cm/s, $n_{p,inj} = 10$ particles/cm^3, and $d_p = 20$ μm for ($+g$), (0-g), and ($-g$) conditions. Simulations included the contributions of Stokes drag and thermophoresis.

The n_p variations can be explained through Eq. 32 which indicates that the n_p is affected by both G_p and $d(u_p)/dx$. More specifically, n_p tends to decrease as G_p increases and as the slope $d(u_p)/dx$ becomes less negative. Physically, a greater G_p indicates more intense radial transport of particles, while a less negative $d(u_p)/dx$ slope indicates less tendency of the particle phase to be "compressed." For very fine particles, e.g., $d_p < 1.0$ μm, the particles follow the gas phase very closely, and in regions in which the gas phase is incompressible (constant density) the particle phase should be also "incompressible," namely, the n_p should be constant. This is reproduced by our simulations in Fig. 3 for the 0.3 μm particles whose n_p is constant except in the zone, which is characterized by rapid thermal expansion. For larger particles that do not follow the gas phase closely, the particle phase can have an apparent "compressibility" (i.e., n_p changes) even in regimes of constant gas phase density. This is shown in Fig. 3 for particles equal to or larger than 5 μm, whose n_p is reduced even in the hydrodynamic zone of the gas phase.

The effect of particle reversal on n_p is shown in Fig. 4 for the $\phi = 0.57$ flame with $u_{exit} = 114$ cm/s, and $d_p = 50$ μm, conditions which result in several motion reversals for the particles. It is apparent that the particle reversal leads to a singular behavior for n_p, which is observed to increase substantially in the vicinity of the PSP's. Mathematically, this is supported by Eqs. 30, 31, and 32. At the PSP's, the spatial derivative of u_p becomes large and can not be balanced by the finite values of G_p, which is independently determined from the radial momentum equation of the particle. The results of Fig. 4 also indicate that as the particles reverse, n_p rapidly drops and that continues in each subsequent reversal until the n_p reaches negligible values. Note that this singular behavior is partially a result of the assumption that particles do not interact with one another. Obviously, the number density is not truly singular but is physically limited by the maximum possible particle packing.

$\frac{du_p}{dx}$

$u_p = \frac{dx}{dt}$

$dt = \frac{dx}{u_p}$

$u_p \to 0.\ dt \to \infty$

accumulati

convected
through
radial
momentum
outward
(sink)

Gravitational effects

The discussion surrounding Eq. 34 indicates that the effect of gravity on the particle dynamics will be substantial for low convective velocities and heavy particles. Simulations were conducted at ($+g$), ($-g$), and (0-g) for the $\phi = 0.25$ flame with $u_{exit} = 14$ cm/s and $d_p = 5$, 10, 20, 50, and 100 μm. Selected results for the particle velocity u_p are shown in Figs. 5 and 6 for $d_p = 20$ and 100 μm, respectively. The results for small (i.e., ≤ 5 μm) particles are not shown as they generally follow the fluid motion and show only a small gravitational effect, only noticeable in the hydrodynamic zone. The devi-

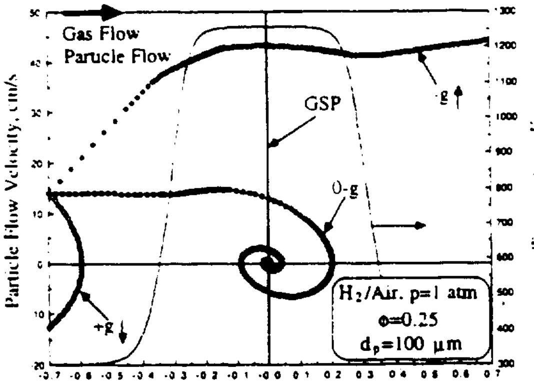

Fig. 6. Gas phase and particle axial velocities profiles for a ϕ = 0.25 H_2/air flame with u_{exit} = 14 cm/s, $n_{p,inj}$ = 10 particles/cm^3, and d_p = 100 μm for $(+g)$, $(0\text{-}g)$, and $(-g)$ conditions. Simulations included the contributions of Stokes drag and thermophoresis. Temperature profile (solid line) indicates flame location.

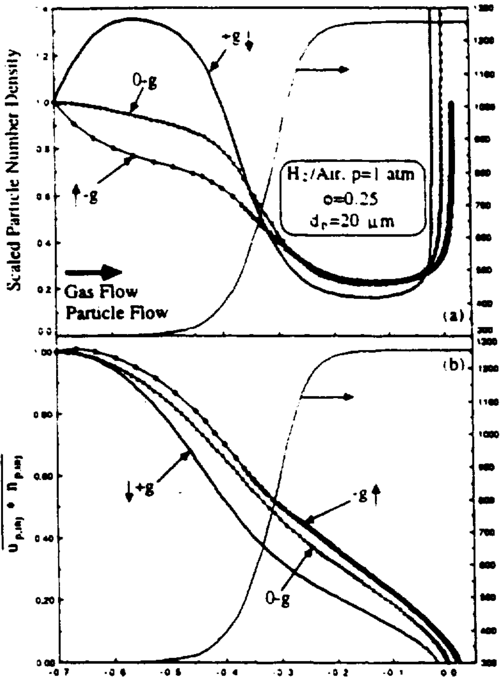

Fig. 7. For a ϕ = 0.25 H_2/air flame with u_{exit} = 14 cm/s, $n_{p,inj}$ = 10 particles/cm^3, and d_p = 20 μm (a) spatial variation of the particle number density scaled by its injection value (b) spatial variation of the product of particle number density times particle axial velocity scaled by its injection value for $(+g)$, $(0\text{-}g)$, and $(-g)$ conditions. Simulations included the contributions of Stokes drag and thermophoresis. Temperature (solid line) profile indicates flame location.

ations disappears in the reaction zone as the increased drag forces, (resulting from the higher gas velocities that accompany the thermal expansion) overwhelm the gravitational forces. The gravitational effect becomes more significant for the 10 and 20 μm particles. For example, Fig. 5 (20 μm particles) depicts that $(+g)$ conditions result in a negative d(u_p)/dx velocity gradient at the nozzle exit; the magnitude of this change can be expected to increase with d_p as the gravitational force increases as $(d_p)^3$ while the drag forces increase proportional to d_p. Thus, the $(-g)$ condition results in a positive d(u_p)/dx gradient at the nozzle exit which again increases with d_p. The results for the $(0\text{-}g)$ conditions indicate that u_p develops initially under the influence of the Stokes drag, as expected.

As also expected, the gravity effect on u_p was found to be even more dramatic for the larger particle diameters of 50 and 100 (Fig. 6) μm, respectively. For both sizes under $(+g)$ conditions, the particles stagnate at a short distance (~1 mm for the present conditions) from the nozzle exit, before even reach the GSP, reverse, and eventually re-enter the nozzle. For $(-g)$ and $(0\text{-}g)$ conditions, however, the picture is different. Figure 6 shows that, at $(0\text{-}g)$ the 100 μm particles penetrate deep into the flowfield, cross the GSP, stagnate inside the opposing jet regime, and subsequently reverse several times until they reach an equilibrium state. Figure 6 also depicts that the large 100 μm particles under the favorable $(-g)$ conditions, possess high enough inertia to shoot through the GSP and reach the opposing nozzle. 6

A direct consequence of the gravity effect is the potentially large modification in the n_p distribution, especially for large particles. This can be especially seen in Fig. 7a for the 20 μm particles, where the substantial discrepancy of the n_p values between the $(+g)$, $(-g)$, and $(0\text{-}g)$ conditions can be easily seen. The $(+g)$ conditions result in particle accumulation at the vicinity of the nozzle exit, while the $(-g)$ conditions result in a substantial reduction of n_p in the same area. This discrepancy was found to be even more apparent for the 50 and 100 μm particles. 7

These observations can partially explain the substantial differences which have been observed for the burning rates of reacting dusty flows under normal- and micro-gravity conditions (e.g., [2]). The presence of gravity can affect the dynamic response of the particles and substantially modify the spatial distribution of the particle mass flux. This can be seen in Fig. 7b, which shows the spatial variation of the product $n_p * u_p$, (which is directly proportional to the particle mass flux) scaled by its injection value, for $(+g)$, $(-g)$, and $(0\text{-}g)$ conditions. For the case of reacting particles, this is translated to a substantial modification of the rate at which (solid) fuel is supplied to the reaction zone and thus one can expect the burning rate to be significantly affected by the gravitational orientation.

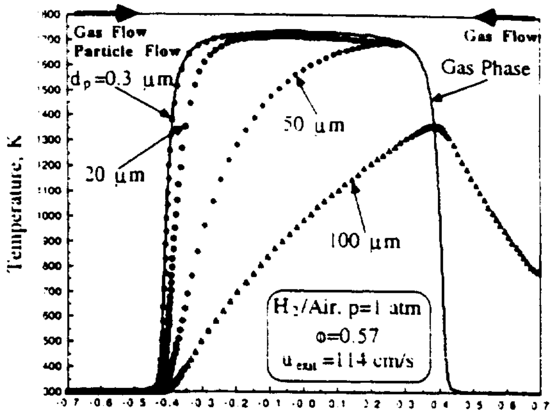

Fig. 8. Gas phase and particle temperatures profiles for a $\phi = 0.57$ H$_2$/air flame with $u_{\text{exit}} = 114$ cm/s, $n_{p,inj} = 10$ particles/cm^3, and $d_p = 0.3, 20, 50$, and 100 μm. Simulations included the contributions of Stokes drag, thermophoresis, and normal gravity $(+g)$.

Thermal Effects on the Particles

The particle thermal response is controlled by its thermal energy equation (Eq. 28). When transformed to an Eulerian frame of reference, it can be shown that the spatial variation of the particle temperature T_p is given by

$$\frac{\mathrm{d}T_p}{\mathrm{d}x} = \frac{A_3}{u_p d_p^2 c_{\text{par}} \rho_{\text{par}}} + \frac{A_4}{u_p d_p c_{\text{par}} \rho_{\text{par}}}, \tag{35}$$

where A_3 and A_4 are combinations of the various parameters contained in Eqs. 26, 28, and 29. The convective-conductive terms have been absorbed in the A_3 parameter, while the radiation terms have been absorbed into the A_4 parameter. Equation 35 indicates that the spatial variation of T_p is inversely proportional to the particle velocity, density, and specific heat. Thus, the higher the values of u_p, ρ_{par}, and c_{par}, the slower is the heating rate of the particle.

Changing the particle diameter d_p has a very different effect on the convective/conductive and the radiative thermal interactions between the two phases. For the convective/conductive interaction, the particle heating rate is inversely proportional to d_p^2 indicating the physical importance of the ratio between the characteristic length for the heat conduction (d_p) between the two phases and the particle volume ($\sim d_p^3$), which is a measure of the particle mass and thus the particle's thermal capacity. For the radiative interaction, the heat transfer rate is inversely proportional to d_p indicating the physical importance of the ratio between the particle surface ($\sim d_p^2$), which affects the total radiative energy transfer, and the particle's thermal capacity which is again proportional to ($\sim d_p^3$).

The effect of d_p on the particle heating is shown in Fig. 8 for the $\phi = 0.57$ flame with $u_{\text{exit}} = 114$ cm/s and $d_p = 0.3, 20, 50$, and 100 μm. It is apparent that the smaller, 0.3 μm particles heat up very quickly and follow the gas phase temperature closely. For the larger particles, a hysteresis exists, which becomes larger as d_p increases. For the 50 μm particles which undergo several reversals, it is of interest to note that during these reversals around the GSP ($x = 0$) the particles eventually are heated up to temperatures which are close to those of the gas phase.

The effect of particle reversal on the particle heating can be seen more clearly in Fig. 9 for the $\phi = 0.57$ flame, with $u_{\text{exit}} = 400$ cm/s and $d_p = 20$ μm. The particles are heated slowly while on the left side of the GSP ($x = 0$). After they penetrate the GSP they reach a local maximum in temperature, and are subsequently rapidly cooled to their initial injection temperature just as they reach the first PSP. This temperature reduction is quite rapid as the particles undergo intense convective cooling by the opposing jet once they penetrate the GSP. Upon reversal, the particles are heated, relatively quickly, back

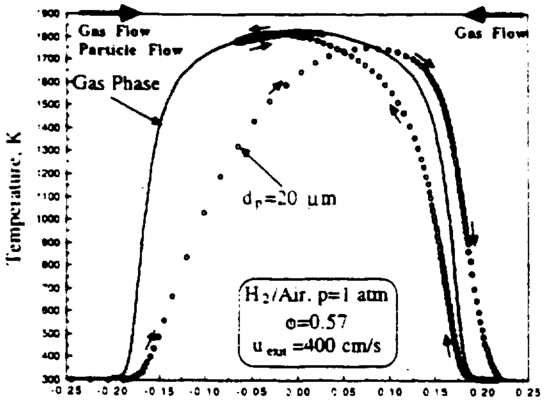

Fig. 9. Gas phase and particle temperatures profiles for a $\phi = 0.57$ H_2/air flame with $u_{exit} = 400$ cm/s. $n_{p,inj} = 10$ particles/cm^3. and $d_p = 20$ μm. Simulations included the contributions of Stokes drag, thermophoresis. and normal gravity ($+g$). Arrows indicate the direction of the particle motion.

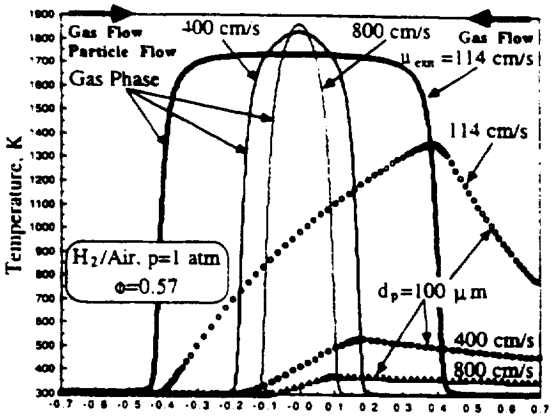

Fig. 10. Gas phase and particle temperatures profiles for a $\phi = 0.57$ H_2/air flame with $u_{exit} = 114$, 400, and 800 cm/s. $n_{p,inj} = 10$ particles/cm^3, and $d_p = 100$ μm. Simulations included the contributions of Stokes drag, thermophoresis, and normal gravity ($+g$).

to temperatures close to those of the gas phase, and as they undergo further reversals around the GSP, they eventually reach a maximum temperature that is close to the maximum gas temperature. Note, that during the first reversal path towards the flame following the first PSP ($x \approx +0.22$ cm), the particles are heated faster as compared to when the particles first enter the preheat zone ($x \approx -0.19$ cm). This occurs because the particle velocity fields are very different in these two regions (as can be seen in Fig. 2a). When the particles first enter the preheat zone, (0.2 cm $< x < 0$ cm), their velocities are of the order of 150 to 250 cm/s while in their first direction reversal (0.12 cm $< x < 0.22$ cm) their velocities range from zero to approximately 120 cm/s in magnitude. Consequently, the returning particles have more time in contact with the heated fluid and more rapidly rise towards the flame temperature.

The effect of the gas and particle injection velocity, u_{exit}, on the particle heating can be further seen in Fig. 10 for the $\phi = 0.57$ flame with $d_p = 100$ μm, and $u_{exit} = 114$, 400, and 800 cm/s. Results show that as u_{exit} increases, the two flames approach the GSP shrinking the region occupied by hot products, but at the same time, the maximum flame temperature increases, as is typical of these Le < 1 flames (e.g., [36]). However, reducing u_{exit} results in heating the particles to higher temperatures. This indicates that the correspondingly larger residence times of the particles in the regions of large gas temperature are more important in determining the particle temperature than an increase of the flame temperature. Thus, for very high u_{exit} (e.g., $u_{exit} = 800$ cm/s), the particle temperature is only slightly modified from its injection value despite the larger flame temperatures.

The effect of gravity on the particle heating is shown in Fig. 11 for large particles and small

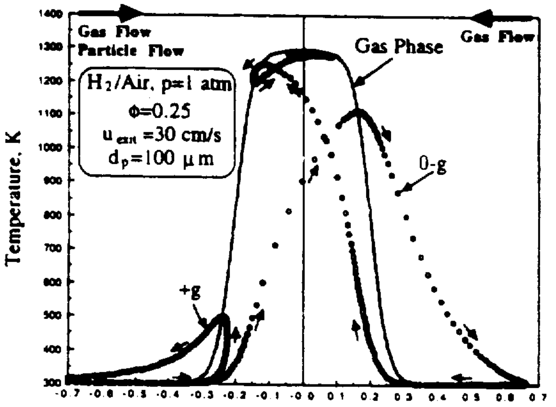

Fig. 11. Gas phase and particle temperatures profiles for a $\phi = 0.25$ H_2/air flame with $u_{exit} = 30$ cm/s, $n_{p,inj} = 10$ particles/cm^3, and $d_p = 100$ μm for ($+g$) and (0-g) conditions. Simulations included the contributions of Stokes drag and thermophoresis. Arrows indicate the direction of the particle motion.

injection velocities ($\phi = 0.25$, $d_p = 100$ μm, and $u_{exit} = 30$ cm/s). For $(+g)$, these heavy particles stagnate well before they reach the GSP and reverse towards the feed nozzle exit. During this excursion, the particles are first heated only to about 500 K, as they do not have a chance to interact with the hotter regions of the flame further downstream. During the return path the particles cool more gradually than the heating generating a hysteretic behavior that reflects the particles' large thermal capacity, which delays both their initial heating and the subsequent cooling. At (0-g), the particles penetrate the GSP and undergo several reversals before settling on the GSP. During these reversals, the particles follow a complex temperature variation as they sequentially interact with hotter and colder gas layers. These results unambiguously show that gravity can have a potentially strong effect on the particle thermal response as well as the particle dynamics.

The relative importance of the various terms of Eq. 28 on the particle thermal state was also analyzed in detail. It was found that the convective/conductive term, Q_p, strongly dominates within the flame zone for all cases studied. Away from the flame zone, the Q_p term was found to be comparable in magnitude to $Q_{g,rad-p}$ as radiation provides a mechanism for long-range interactions with the high temperature regions of the flow. The particle radiation term, $Q_{p,rad}$, was found to be maximum at the vicinity of maximum T_p, as it is expected, but in such regions its contribution is substantially lower than that of Q_p.

Dynamic and Thermal Effects on the Gas Phase

For low particle number density n_p, the dynamics and thermal response of the gas phase are nearly unaffected by the presence of particles. This was the case for all the results which were shown in Figs. 1 through 11. For these simulations, the low value of $n_{p,inj} = 10$ particles/cm^3 was chosen in order to isolate the particle effects from the gas-phase effects. However, as n_p increases, the gas phase can be affected by the presence of the particles both dynamically and thermally, as should be apparent from Eqs. 24 and 25, respectively.

The dynamic coupling results from the forces which develop between the two phases and thus can affect the momentum balance of the gas phase and the gas phase velocity field. This possibility was assessed for the $\phi = 0.57$ flame, with $u_{exit} = 400$ cm/s, $d_p = 50$ μm, and $n_{p,inj} = 5800$ particles/cm^3. The simulations were conducted with and without the particle-gas force interaction in Eq. 28. It was found that if the particles penetrate the GSP, they can affect u_g especially in a region just to the right of the GSP. Thus, by allowing the particle-gas interaction, u_g becomes lower in magnitude. Physically, this is a result of the force exerted between the two phases, which reaches a maximum just to the right of the GSP where the relative velocity between the phases, and thus the interphasial drag forces, are at a maximum. As a consequence, the gas experiences a force of equal magnitude and opposite sign to that experienced by the particles, resulting in a reduction of the magnitude of u_g.

The thermal effects on the gas phase was found to be significant as n_p increases. More specifically, by injecting particles at ambient temperature, the flames are cooled, and, as $n_{p,inj}$ is gradually increased, near-extinction conditions were observed. The cooling effect was found to be stronger for the left flame of the twin-flame assembly, as the left flame interacts first with the incoming cold particles (which are only injected from the left jet). It was also shown, that this cooling effect was different for particles with small and large inertia, as the particles with large inertia penetrate deeper into the flowfield and can interact thermally with both jets.

The temperatures of the gas, T_g, and particles, T_p, are shown in Fig. 12 for the $\phi = 0.57$ flame, with $u_{exit} = 114$ cm/s, $d_p = 20$ μm, and $n_{p,inj} = 10$ and 24,500 particles/cm^3. It can be seen that for the higher $n_{p,inj}$, T_g is substantially reduced for the left flame, while the temperature of the right flame is nearly unaffected. For the higher $n_{p,inj}$, T_p is also reduced as a result of the reduction in flame temperature.

In Figs. 13 and 14 results are shown for the $\phi = 0.57$ flame, with $u_{exit} = 400$ cm/s and $d_p = 50$ μm. For this case, the particle inertia is large enough that the particles can reach all the way to the opposing nozzle exit and thus, thermally

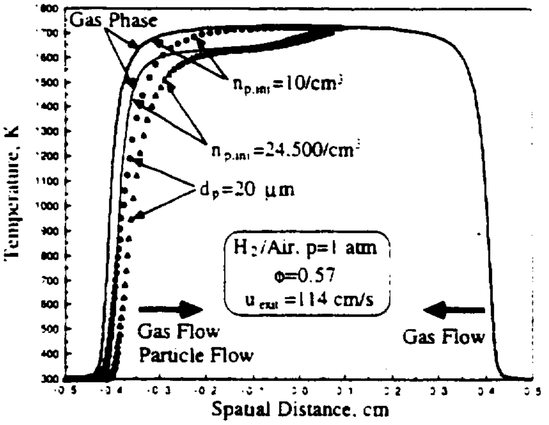

Fig. 12. Gas phase and particle temperatures profiles for a $\phi = 0.57$ H_2/air flame with $u_{exit} = 114$ cm/s. $n_{p,inj} = 10$ and 24.500 particles/cm^3. and $d_p = 20$ μm. Simulations included the contributions of Stokes drag, thermophoresis, and normal gravity ($+g$).

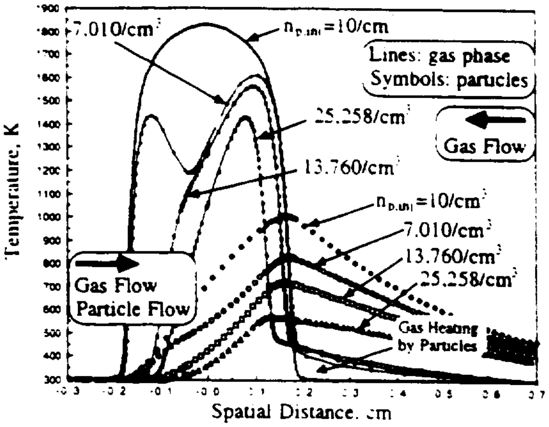

Fig. 14. Gas phase and particle temperature profiles for a $\phi = 0.57$ H_2/air flame with $d_p = 50$ μm. $u_{exit} = 400$ cm/s. and $n_{p,inj} = 10$. 7.010. 13.750. and 25.258 particles/cm^3. Simulations included the contributions of Stokes drag, thermophoresis, and normal gravity ($+g$).

affect the entire flowfield. The dependence of the maximum flame temperature, $T_{f,max}$, on $n_{p,inj}$ can be seen in Fig. 13: for all $n_{p,inj}$'s. $T_{f,max}$ is the maximum temperature of the right flame as the left flame undergoes more intense cooling. As expected, the results of Fig. 13 indicate that $T_{f,max}$ is first monotonically reduced with $n_{p,inj}$. It was found that the left flame is extinguished for $n_{p,inj} = 13{,}450$ particles/cm^3, while a "turning-point" behavior is observed at $n_{p,inj} = 26.627$ particles/cm^3. which indicates extinction of the right flame as well and as a consequence global extinction. This "turning-point" extinction behavior is typical of flames undergoing cooling and it could be captured by the one-point continuation technique that was implemented in this model.

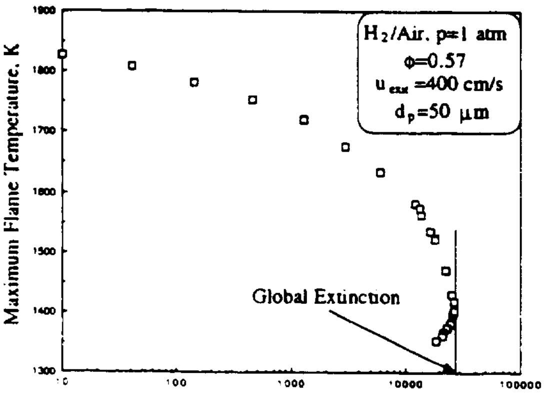

Fig. 13. Maximum flame temperature variation with particle number density, for a $\phi = 0.57$ H_2/air flame with $u_{exit} = 400$ cm/s. and $d_p = 50$ μm. Simulations included the contributions of Stokes drag, thermophoresis, and normal gravity ($+g$).

Figure 14 shows the thermal structures of the gas and particle phases for three of the cases in Fig. 13: for $n_{p,inj} = 10$, 7.010, 13.760, and 25,258 particles/cm^3. For $n_{p,inj} = 10$ particles/cm^3 case, T_g is unaffected by the particles, while for the $n_{p,inj} = 7{,}010$ particles/cm^3 case, T_g is substantially reduced throughout the flame assembly with, as would be expected, a more profound effect on the left side of the flame assembly that first encounters the particles. T_p is also smaller than the $n_{p,inj} = 10$ particles/cm^3 case, again reflecting the reduction in flame temperature. Thus, these particles remove thermal energy from the high-temperature regions of the gas phase and transfer that energy to other parts of the flowfield, preheating the gas flow coming from the right nozzle. This can be seen in Fig. 14, as the gas phase temperature of the jet emerging from the right nozzle, starts increasing well ahead of the flame reflecting the preheating induced by the heated particles. The $n_{p,inj} = 13{,}760$ particles/cm^3 case describes a state just after the left flame has been extinguished, and results for both the gas and particle phases reflect the existence of only a single flame. The $n_{p,inj} = 25{,}258$ particles/cm^3 case describes a state just before the right flame extinction, (i.e., when both flames are extinguished). The substantial reduction of the temperatures of both phases is apparent.

Finally, it should be noted that for all studies on the effect of $n_{p,inj}$ on the gas phase, special care was taken to account for the local n_p modification when particle reversal(s) was(were) observed. Thus, the effective n_p which was used in the gas energy equation, was obtained by summing over the contributions to n_p resulting by all reversal paths.

CONCLUSIONS

In the present study, the dynamic and thermal interactions between inert Al_2O_3 particles and strained, laminar, premixed H_2/air flames were numerically investigated in a stagnation flow configuration. In this analysis, the quasi-one-dimensional conservation equations that describe the ideal stagnation flow for the gas phase were solved. These equations include the particle-gas phase force interaction in the momentum equation, and detailed description of chemical kinetics and molecular transport. A set of conservation equations was also developed for the particles in ideal stagnation flows. The particle momentum balance included the effects of thermophoresis and gravity in addition to the Stokes drag force. The particle thermal energy balance included convective/conductive and radiative exchanges between the particle and the surrounding gas. A one-point continuation approach was also implemented, allowing for the determination of singular, turning points, describing flame extinction. The effects of the gas phase stoichiometry, strain rate, particle inertia, thermophoresis, and gravity were assessed.

As expected, results show that while small, submicron particles follow the gas phase closely, larger particles fail to do so. For the small particles, the effect of thermophoresis was found to be significant in regions of large temperature gradients in the gas phase, an effect that was not as important for large particles. This is in agreement with results of previous studies. Particles possessing large inertia were found to penetrate the GSP, stagnate in the counterflow the opposing jet, and subsequently reverse direction several times around the GSP, in agreement with previously observed flow reversal for droplets in stagnation-type flows. Finally, the results demonstrate that the parameters affecting the particle velocity can also directly affect the particle number density which varies significantly throughout the flowfield.

Simulations at $(+g)$, $(0\text{-}g)$, and $(-g)$ showed that the magnitude and direction of the gravitational force can have a strong effect on heavy particles moving at low velocities. In addition to significantly modifying the particle velocity field, gravity was also found to be responsible for the modification of the particle temperature, number density, and mass flux distribution, which may partially explain experimentally observed effects of gravity on flame propagation in dusty reacting flows.

The thermal effects between the two phases were also found to be strong. Results show that the particle heating rate is lower for high-inertia particles. Under conditions that result in particle flow reversal, the particle temperature was shown to vary in a highly non-monotonic manner, by interacting with gas layers of vastly different temperatures.

Finally, simulations with high particle number densities showed that the presence of the particles can affect both the velocity and temperature fields of the gas phase. The velocity field was found to be affected because of the forces that develop between the two phases. The effect on the gas phase temperature is mainly a result of the heat transfer between the hot flame and the cold particles. As the number density increases, the flames can be cooled to extinction states. Under conditions of high particle inertia, the heated particles can penetrate deep into the opposing jet, and for very high values of the number density can cause an "early" preheating of the incoming gas.

This work was supported by NASA under grant NAG3-1877. Special thanks to our technical monitor Dr. Randall Vander Wal.

REFERENCES

1. Faraday, M., and Lyell, C., Report to the Home Secretary on the Explosion at the Haswell Colliery on 28 Sept. 1844; also Phil. Mag. 26, p. 16 (1845).

2. Kobayashi, H., Ono, N., Okuyama, Y., and Niioka, T., *Twenty-Fifth Symposium (International) on Combustion*, Combustion Institute, Pittsburgh, 1994, pp. 1693–1699.
3. Ballal, D. R.: *Proc. R. Soc. Lond.* A 385:21–51 (1983).
4. Continillo, G., and Sirignano, W. A., *Combust. Flame* 81:325–340 (1990).
5. Chen, N.-H., Rogg, B., and Bray, K. N. C., *Twenty-Fourth Symposium (International) on Combustion*, Combustion Institute, Pittsburgh, 1992, pp. 1513–1521.
6. Gutheil, E., and Sirignano, W. A., *Combust. Flame* 113:92–105 (1998).
7. Graves, D. B., and Wendt, J. O. L., *Nineteenth Symposium (International) on Combustion*, Combustion Institute, Pittsburgh, 1982, pp. 1189–1196.
8. Chen, G., and Gomez, A., *Twenty-Fourth Symposium (International) on Combustion*, Combustion Institute, Pittsburgh, 1992, pp. 1531–1539.
9. Gomez, A., and Rosner, D. E., *Combust. Sci. Tech.* 89:335–362 (1993).
10. Sung, C. J., Law, C. K., and Axelbaum, R. L., *Combust. Sci. Tech.* 99:119–132 (1994).
11. Sung, C. J., Kistler, J. S., Nishioka, M., and Law, C. K., *Combust. Flame* 105:189–201 (1996).
12. Xing, Y., Köylü, Ü., and Rosner, D. E., *Combust. Flame* 107:85–102 (1996).
13. Marble, F. E., *Ann. Rev. Fluid Mech.* 2:397–446 (1970).
14. Hjelmfelt, A. T., Jr., and Mockros, L. F., *Appl. Sci. Res.* 16:149–161 (1966).
15. Allen, M. D., and Raabe, O. G., *Aerosol Sci. Technol.* 4:269 (1985).
16. Kennard, E. H., Kinetic Theory of Gases, McGraw-Hill, New York, 1983.
17. Hirschfelder, J. O., Curtiss, C. F., and Bird, R. B., *Molecular Theory of Gases and Liquids*, Wiley, New York, 1954.
18. Shook, C. A., and Roco, M. C., *Slurry Flow: Principles and Practice*, Butterworth-Heinemann (1991).
19. Brock, J. R., *J. Colloid Sci.*, 17:768 (1962).
20. Talbot, L., Cheng, R. K., Schefer, R. W., and Willis, D. R., *J. Fluid Mech.* 101:737–758 (1980).
21. Waldmann, L., in *Rarefied Gas Dynamics* (L. Talbot, Ed.), Academic, New York, 1961, p. 323.
22. Kee, R. J., Miller, J. A., Evans, G. H., and Dixon-Lewis, G., *Twenty-Second Symposium (International) on Combustion*, Combustion Institute, Pittsburgh, 1988, pp. 1479–1494.
23. Clift, R., Grace, J. R., and Weber, M. E., *Bubbles, Drops and Particles*, Academic Press, New York, 1978.
24. Siegel, R., and Howell, J. R., *Thermal Radiation Heat Transfer*, Hemisphere Publishing Corporation, 1981.
25. Williams, F. A., *Combustion Theory*, Second Edition, Benjamin/Cummings, Inc., Menlo Park, CA, 1985.
26. Nishioka, M., Law, C. K., and Takeno, T., *Combust. Flame* 104:328–342 (1996).
27. Bowman, C. T., Frenklack, M., Gardiner, W., and Smith, G., The GRI mechanism. Personal communications (1995).
28. Kee, R. J., Warnatz, J., and Miller, J. A., A FORTRAN Computer Code Package for the Evaluation of Gas-Phase Viscosities, Conductivities, and Diffusion Coefficients. Sandia Report SAND83-8209, 1983.
29. Tien, C. L., *Advances Heat Transfer* 5:253 (1967).
30. Hubbard, G. L., and Tien, C. L., *ASME J. Heat Transfer* 100:235 (1978).
31. Law, C. K., and Egolfopoulos, F. N., *Twenty-Fourth Symposium (International) on Combustion*, Combustion Institute, Pittsburgh, 1992, pp. 137–144.
32. Egolfopoulos, F. N., *Twenty-Fifth Symposium (International) on Combustion*, Combustion Institute, Pittsburgh, 1994, pp. 1375–1381.
33. Rosenow, W. M., Hartnett, J. P., and Ganic, E. N., *Handbook of Heat Transfer Fundamentals*, McGraw-Hill, New York, 1985.
34. Egolfopoulos, F. N., and Campbell, C. S., *J. Fluid Mech.*, 318:1–29 (1996).
35. Kee, R. J., Rupley, F. M., and Miller, J. A., Chemkin-II: A Fortran Chemical Kinetics Package for the Analysis of Gas-Phase Chemical Kinetics. Sandia Report SAND89-8009, 1989.
36. Law, C. K., *Twenty-Second Symposium (International) on Combustion*, Combustion Institute, Pittsburgh, 1988, pp. 1381–1402.

Received February 10, 1997; revised June 23, 1998; accepted July 9, 1998